Majer, Piotr; Mohr, Peter N. C.; Heekeren, Hauke R.; Härdle, Wolfgang Karl

Working Paper

Portfolio decisions and brain reactions via the CEAD method

SFB 649 Discussion Paper, No. 2014-036

Provided in Cooperation with:
Collaborative Research Center 649: Economic Risk, Humboldt University Berlin

SFB 649 Discussion Paper 2014-036

Portfolio Decisions and Brain Reactions via the CEAD method

Piotr Majer*
Peter N.C. Mohr**
Hauke R. Heekeren**
Wolfgang K. Härdle*

* Humboldt-Universität zu Berlin, Germany
** Freie Universität Berlin, Germany

This research was supported by the Deutsche Forschungsgemeinschaft through the SFB 649 "Economic Risk".

http://sfb649.wiwi.hu-berlin.de
ISSN 1860-5664

SFB 649, Humboldt-Universität zu Berlin
Spandauer Straße 1, D-10178 Berlin

SFB 649 ECONOMIC RISK BERLIN

Portfolio Decisions and Brain Reactions via the CEAD method*

Piotr Majer[†], Peter N.C. Mohr[‡], Hauke R. Heekeren[§], Wolfgang K. Härdle[¶]

Abstract

Decision making can be a complex process requiring the integration of several attributes of choice options. Understanding the neural processes underlying (uncertain) investment decisions is an important topic in neuroeconomics. We analyzed functional magnetic resonance imaging (fMRI) data from an investment decision (ID) study for ID-related effects. We propose a new technique for identifying activated brain regions: Cluster, Estimation, Activation and Decision (CEAD) method. Our analysis is focused on clusters of voxels rather than voxel units. Thus, we achieve a higher signal to noise ratio within the unit tested and a smaller number of hypothesis tests compared with the often used General Linear Model (GLM). We propose to first conduct the brain parcellation by applying spatially constrained NCUT spectral clustering. The information within each cluster can then be extracted by the flexible DSFM dimension reduction technique and finally be tested for differences in activation between conditions. This sequence of Cluster, Estimation, Activation and Decision admits a model-free analysis of the local BOLD signal. Applying a GLM on the DSFM-based time series resulted in a significant correlation between the risk

*The authors greatfully acknowledge financial support from the Deutsche Forschungsgemeinschaft through SFB 649 ”Economic Risk” and IRTG 1792 ”High Dimensional Non Stationary Time Series”.

†Humboldt-Universität zu Berlin, C.A.S.E. - Center for Applied Statistics and Economics, Spandauer Str. 1, 10178 Berlin, Germany, tel: +49 (0)30 2093 5623, fax: +49 (0)30 2093 5649

‡Department of Education and Psychology, Freie Universität Berlin, Berlin

§Department of Education and Psychology, Freie Universität Berlin, Berlin

¶Humboldt-Universität zu Berlin, C.A.S.E. - Center for Applied Statistics and Economics, Spandauer Str. 1, 10178 Berlin, Germany and School of Business, Singapore Management University, 50 Stamford Road, Singapore 178899

of choice options and changes in fMRI signal in the anterior insula (aINS) and DMPFC. Additionally, individual differences in decision-related reactions within the DSFM time series predicted individual differences in risk attitudes as modeled with the framework of the mean-variance model.

Keywords: risk, risk attitude, fMRI, decision making, neuroeconomics, semiparametric model, factor structure, brain imaging, spatial clustering, inference on clusters, CEAD method
JEL classification: C3, C6, C9, C14, D8

1 Introduction

Economic decision making takes place when, for example, an individual buys beverages in a supermarket, purchases a car or chooses an investment fund. Some of these choices are made when the outcome is uncertain and hard to anticipate, which is particularly true for an investment decision. The decision-making process builds on different mechanisms such as representation and integration of relevant evidence for and a comparison process of different choice options. This mechanism has attracted considerable attention in many different fields, from cognitive psychology, behavioral economics, to neuroscience, see, e.g., Glimcher and Fehr (2013). Economic decisions are usually explained in a value-based scheme, where different choice options are evaluated and the option with the highest value is chosen. The values attributed to different incarnations of options may be generated by a nonobservable utility function. It was first formalised by Bernoulli (1738) and further developed by von Neumann and Morgenstern (1953) and Kahneman and Tversky (1979) to address the uncertainty of outcomes. In this case individual risk preferences are attributed to the curvature of the utility function. Alternatively, decision making can be explained in a framework of risk-return models, which incorporate the risk attitude as a weighting factor, see, e.g., Weber and Milliman (1997).

Research in the field of Decision Neuroscience (as well as its sub-field Neuroeconomics) attempts to address human economic behavior (i.e., decisions) by looking at neural systems that underlie decision making (e.g., Camerer (2007); Heekeren et al. (2008)). In practice one measures changes in brain activity using methods such as electroencephalography (EEG) and functional magnetic resonance imaging (fMRI), see, e.g., Ruff and Huettel (2013). FMRI is based on measuring the blood-oxygen-level-dependent (BOLD) signal and captures parameters related to changes in blood flow and blood oxygenation. FMRI data are recorded over time, for example during multiple investment decisions. The captured changes in fMRI BOLD signal are indirectly related to neural firing rates (Logothetis, 2008). The acquired images are high-dimensional and detecting stimulus-related effects is a non-trivial task. Changes in brain activation in response to decision making may be of a modest size (i.e., in comparison to reactions to visual or auditorial stimuli) and possible hemodynamic responses may be subtle and hardly detectable in the BOLD signal. It poses a genuine challenge to all existing methods and may require some extraordinary techniques.

A benchmark method to detect brain regions activated by the stimulus is the general linear model (GLM). GLM is a single-voxel technique which tests each voxel separately and results in a 3-D map of changes in fMRI signal. The test is done in a linear regression setup, where the voxel time series are modeled according to the hypothesized and predefined regressors (design matrix), which correspond to the experimental paradigm and potential confounds. This simple methodology has proved to be extremely successful in practice and has led to a wealth of important findings (e.g., Kable and Glimcher (2007)), also regarding investment decisions (Mohr, Biele, Krugel, Li and Heekeren, 2010; Mohr, Biele and Heekeren, 2010). Nevertheless, it has several limitations. Firstly, all neural activity not predefined in the design is neglected and cannot be identified by the model. In contrast to this model-based approach, recently introduced model-free approaches (Beckmann and Smith, 2005; van Bömmel et al., 2013) offer to identify effects without any a priori hypothesis. Secondly, possible information reflected in variability and higher moments of the BOLD signal (Mohr and Nagel, 2010; Garrett et al., 2013) is disregarded by the GLM approach. Moreover, activation maps derived by the single-voxel approach may by "inherently limited" by a typically low signal to noise ratio of individual voxel data, as reported by Heller et al. (2006). Alternatively, a simultaneous analysis of multi-voxel data that co-vary with the experimental design may increase the signal without adding noise.

To overcome these shortcomings we follow the idea of Heller et al. (2006) and focus our analysis on the cluster rather than voxel unit. This leads in fact to an alternative technique for analyzing fMRI data, where the brain parcellation serves as a starting point. The fMRI clustering is done by the normalized cut spectral algorithm (Shi and Malik, 2000) which became very popular in neuroscience, see, e.g., Craddock et al. (2012). The algorithm makes use of a correlation between neighboring voxels which defines their proximity. Thus, a possible co-movement (i.e., simultaneous hemodynamic response) plays a key role in defining a homogeneous cluster. The shape and spatial structure is data-driven and clusters are contiguous volumes of voxels, ensuring interpretability. After functional connectivity maps are constructed one needs to investigate neural activity displayed by the cluster unit. Our approach is model-free, the signal carried within a cluster is extracted by the dynamic semiparametric factor model (DSFM). The DSFM, proposed by Park et al. (2009), is employed here as a dimension reduction technique (van Bömmel et al., 2013). It filters the noise and extracts only the common temporal information (i.e., joint reaction by neighboring voxels to the stimulus). The resulting simple, denoised temporal representation of cluster dynamics may be tested for activation within the GLM framework or using a model-free approach. Our technique: Cluster, Estimation, Activation and Decision (CEAD) method combines parcellation based on functional connectivity and DSFM. Thus, it greatly simplifies the complexity of the data while preserving the high accuracy of the representation. Particularly this high spatiotemporal accuracy is of great importance, when stimulus related effects may be subtle and local (such as in investment decisions under risk).

The presented methodology is applied to investigate a possible relationship between individual differences in risk preferences and dynamics in the BOLD response. In the first step the extracted temporal information from clusters is tested for changes in brain activation. These, possibly few, activated clusters correlated with risk are further investigated with respect to risk attitudes estimated from subject responses to ID tasks. Here, we establish a link between changes in BOLD signal and individuals' risk weights in a risk-return model. Based on this analysis we identify bilateral anterior insula (aINS) activity as a correlate of risk (standard deviation). The risk attitudes, derived from the subject's investment decisions are successfully predicted based only on underlying brain activity in aINS.

In the upcoming section (2) we describe the experimental procedures, our methodology and derivation of risk attitudes. At the end of that part a short simulation study of testing performance is shown. In the next section (3) our modeling parameters and empirical findings are reported. We show and exploit the relation between risk preferences and temporal information extracted from clusters. Our conclusions are detailed in the discussion section.

2 Materials and Methods

In this section our experimental and fMRI data acquisition setup is presented. In the next step we describe our methodology and employed statistical tools. It begins with an introduction to the normalized cut spectral clustering (NCUT). Secondly, the advanced dimension reduction technique: DSFM is discussed. It shows how to extract a temporal information (i.e., hemodynamic reponse) from entire clusters. We briefly sketch our activation testing procedure which is similar to the voxelvise GLM approach. The testing performance is evaluated in a simulation study. Finally, we introduce the risk-return model and estimate the subjects' risk attitudes based on their investment decisions.

2.1 Experimental Procedures

Subjects, $I = 19$, performed an adjusted version of the Risk Perception in Investment Decisions (RPID) Task (Mohr, Biele, Krugel, Li and Heekeren, 2010). In this task subjects see past returns of either one single investment or two investments that form a portfolio (50% of the money invested in each). While they see the past returns they have to make a choice between, if they would prefer to invest in a bond with 5% fixed return or the investment that is displayed (either single risky investment or risky portfolio). The choice situations differed in three within-subject conditions: (A) choices between 5% fixed return and a single risky investment, (B) choices between 5% fixed return and a risky portfolio of 2 single investments with perfectly ($\rho = 1$) correlated returns, and (C) choices between 5% fixed return and a risky portfolio of 2 single investments with uncorrelated returns ($\rho = 0$). Importantly, the return history of the risky options (either single investment or portfolio) was exactly the same in all 3 conditions. All displayed returns were gaussian with different set of parameters μ and σ, where $\mu = 5\%, 7\%, 9\%, 11\%$ and $\sigma = 2\%, 4\%, 6\%, 8\%$. Each of the choices regarding single investments was repeated once to hold the number of choices between the bond and a single investment and the bond and a portfolio constant. In total subjects made 256 choices in two blocks of 128 choices each. Subjects had a maximum of 7 seconds to enter their choices via a response box with two buttons. The location of the choice options on the screen was counterbalanced between left and right to avoid order effects.

2.2 fMRI Data

MRI data were acquired on a 3 T scanner (Trio; Siemens) using a 12-channel head coil. Functional images were acquired with a gradient echo T2*-weighted echo-planar sequence (TR = 2000 ms, TE = 30 ms, flip angle = 70, 64×64 matrix, field of view = 192 mm, voxel size = $3 \times 3 \times 3$ mm^3). A total of 37 axial slices (3 mm thick, no gap) were sampled for whole-brain coverage. Imaging data were acquired in two functional runs with 695 and

705 volumes respectively. A high-resolution T2-weighted anatomical scan of the whole brain was acquired (256×256 matrix, voxel size $= 2 \times 2 \times 2$ mm^3).

The data was initially pre-processed with FSL 4.0 (FMRIB's Software Library). Pre-processing included motion correction and slice-time correction. Additionally, images were normalized into a standard stereotaxic space (Montreal Neurological Institute (MNI), Montreal, Quebec, Canada). As a result high-dimensional data was obtained $91 \times 109 \times 91 \times 1400$, where $t = 1, \ldots, 1400$ for each subject $i = 1, \ldots, 19$.

2.3 fMRI Analysis

The key idea of this study is to use data-driven, contiguous clusters as the units of the analysis. The clustering is done by a Spatially Constrained Spectral Clustering algorithm which became extremely successful in neuroscience, see, e.g., Craddock et al. (2012). In the second step, temporal information contained in each cluster is extracted by the DSFM approach, as am alternative to averaging over voxels in the clusters proposed by Heller et al. (2006). Comparison with the latter approach is presented in a simulation study (see section 2.4) and our empirical results. After the cluster temporal information is extracted, activated regions of interest (ROIs) are found by the GLM testing procedure.

2.3.1 Spatially Constrained Spectral Clustering

The brain parcellation results from normalized cut spectral clustering (NCUT). This technique, first proposed by Shi and Malik (2000), is reported to be robust to outliers (Luxburg, 2007) and computationally efficient. It also allows for a simple incorporation of constraints, i.e., a spatial contiguousness, which can be exploited in the human brain mapping. The method was introduced to the field of cognitive neuroscience by van den Heuvel et al. (2008); Shen et al. (2010); Craddock et al. (2012). Shen et al. (2010) reported that task-related fMRI data may be analyzed with this algorithm and that the resulting brain parcellation is highly consistent with the resting-state fMRI. The NCUT approach is closely related to the graph theoretic formulation of clustering. The set of voxels $Y = (Y_1, \ldots, Y_J)$ is represented as a weighted undirected graph, where the nodes of the graph are the voxels and an edge is given between every pair of voxels Y_j and $Y_{j'}$. The weight on each edge, denoted by $w(j, j')$, is a proximity measure between voxels (nodes) j and j', and is defined as in the previous paper:

$$w(j, j') = \begin{cases} \max\{\mathrm{Corr}_t(Y_j, Y_{j'}), 0\} & , \text{for } \|X_j - X_{j'}\| < d, \\ 0 & , \text{otherwise}, \end{cases} \tag{1}$$

where $\|\cdot\|$ denotes the Euclidean norm in $\mathbb{R}^3$ space, $X_j \in \mathbb{R}^3$ are j-th voxel coordinates. The radius d is selected in such a way that only the 26 nearest neighbors (face and edge touching; 3-D neighborhood of a single voxel) are included. Such a constraint ensures a contiguous shape of each cluster (Xu et al., 2005; Kamvar et al., 2003). Moreover, the similarity matrix $W = \{w(j, j')\}_{j,j'=1,\ldots,J}$ (of size $J \times J$) derived by (1) is sparse and thus computational complexity is reduced. The similarity between voxels in 3-D neighborhood is given by correlation coefficient of the voxels time series with a threshold to make it non-negative. By applying the correlation as a similarity measure we ensure the temporal homogeneity within a cluster, which is further exploited in the next section (2.3.2). Once a proximity measure is chosen, a group-building algorithm for creating a functional connectivity map needs to be specified. The NCUT algorithm is a hierarchical procedure, it starts with the coarsest partition possible: one cluster contains all of the voxels. It proceeds by splitting the single cluster up into smaller sized clusters until a pre-specified number of groups C is achieved. The partition of an initial set is done such that the similarity between voxels within the proposed group is greater than the similarity between voxels in different groups. For example, for two disjoint groups P and Q, one computes the normalized cut cost by:

$$N_{cut}(P, Q) = \frac{\sum_{Y_j \in P, Y_{j'} \in Q} w(j, j')}{\sum_{Y_j \in P, Y_{j'} \in R} w(j, j')} + \frac{\sum_{v_j \in P, Y_{j'} \in Q} w(j, j')}{\sum_{Y_j \in Q, Y_{j'} \in R} w(j, j')}, \tag{2}$$

where $R = Q + P$ is the initial set that has to be partitioned. The denominators in the formula (2) may be seen as a sum of all similarities between sets P and Q that are neglected in this division. The nominators stand for all the similarities between the proposed groups (P and Q) and the initial set R, thus a size of a group has an influence on the normalized cut cost. Finding an optimal division of set R might be found by minimizing the normalized cut criterion:

$$(P^*, Q^*) = \arg \min_{R=P+Q} N_{cut}(P, Q). \tag{3}$$

Therefore we ensure that, simultaneously, similarities within each cluster are maximized and similarities between clusters are minimized. This approach leads to balanced sizes of clusters and reduces the likelihood of obtaining singletons as a result. Shi and Malik (2000) showed that minimizing (2) is equivalent to minimizing the Rayleigh quotient denoted by:

$$Q(y) = \frac{y^\top \mathcal{L} y}{y^\top D y}, \tag{4}$$

under the constraint that y is a piecewise (discrete) vector $J \times 1$ and $y^\top \operatorname{diag}(D) 1_J = 0$. Matrix $\operatorname{diag}(D)$ is defined by $D = (d_1, \ldots, d_J)$ a degree vector, $d_j = \sum_{j'=1}^{J} w(j, j')$ and $\mathcal{L}$ is the Laplacian of the graph given by:

$$\mathcal{L}(j, j') = \begin{cases} d_j & , \ j = j', \\ -w(j, j') & , \ w(j, j') > 0, \\ 0 & , \ \text{elsewhere.} \end{cases} \tag{5}$$

Minimizing the formula (4) is closely related to spectral clustering, where the first non-trivial eigenvector of the graph Lapacian matrix $\mathcal{L}$ is used. The authors showed that the problem is NP-complete, an approximate discrete solution can be found efficiently.

2.3.2 Dynamic Semiparametric Factor Model

The clusters are constructed to maximize the temporal homogeneity between voxels. Their similar time evolution (i.e., reflected in joint hemodynamic response after stimuli) explicitly suggest possible low-dimensional representation of the multidimensional time series. The temporal variability in the cluster series, that may be related to investment decisions and possibly individual differences in risk attitude, is captured by a dynamic semiparametric factor model (DSFM), proposed by Park et al. (2009). DSFM serves here as a dimension reduction technique, which is able to extract temporal dynamics from the functional connectivity brain maps by corresponding low dimensional time series (factor loadings) in only one estimation step. Due to a subject-specific spatial structure of the brain functional connectivity maps, we model each cluster separately.

The BOLD signal of all voxels in a single cluster c, $c = 1, \dots, C$ during the entire experiment is a multi-dimensional time series. The stated below DSFM is designed to model such high-dimensional time series:

$$\begin{aligned} Y_{t,j} &= m_0(X_{t,j}) + \sum_{l=1}^{L} Z_{t,l}\, m_l(X_{t,j}) + \varepsilon_{t,j}, \;\; 1 \le j \le J_c, \; 1 \le t \le T. \\ &\overset{\text{def}}{=} Z_t^\top m(X_{t,j}) + \varepsilon_{t,j} = Z_t^\top A^* \Psi_{t,j} + \varepsilon_{t,j}, \end{aligned} \tag{6}$$

where $Z_t = (\mathbf{1}, Z_{t,1}, \dots, Z_{t,L})^\top$ is a latent $(L+1)$-dimensional stochastic process and m is an $(L+1)$-tuple $(m_0, \dots, m_L)$ of unknown real-valued functions m_l. More precisely, the voxel's coordinates $(x_1, x_2, x_3) \in \mathbb{R}^3$ that belongs to an analyzed cluster c is the covariate $X_{t,j}$ (in this setup it is time-invariant $X_{t,j} = X_j$) and the normalized BOLD signal is the dependent variable $Y_{t,j}$; $j = 1, \dots, J_c$; $t = 1, \dots, T$. We assume $\varepsilon_{t,j} \perp Z_{t,j}$, $\mathsf{E}\,\varepsilon_{t,j} = 0$ and $\mathsf{E}\,\varepsilon_{t,j}^2 < \infty$. The functions m_l are given as a linear combination of space basis functions $\Psi_{t,j} = [\psi_1(X_{t,j}), \dots, \psi_K(X_{t,j})]^\top$ and corresponding $(L+1) \times K$ matrix of unknown coefficients A^*. In our setup, $[\psi_1(X_{t,j}), \dots, \psi_K(X_{t,j})]^\top$ are quadratic tensor B-splines on K equidistant knots. To find the estimates of $Z_t^\top$ and A^* one solves:

$$(\widehat{Z}_t, \widehat{A^*}) = \arg\min_{Z_t, A^*} \sum_{t=1}^{T} \sum_{j=1}^{J} \{Y_{t,j} - Z_t A^* \Psi_{t,j}\}^2 \,. \tag{7}$$

A solution to the problem stated in (7) may be found by the Newton-Raphson method. Time dynamics are represented by $\widehat{Z}_t$, while $\widehat{A^*}$ captures the smooth, nonparametrically estimated spatial structure of clusters.

In the formula (6) the time frame is constant over all clusters and equals $T = 1400$. Due to varying spatial structure and size of each cluster c, $c = 1, \dots, C$, we denote the dimension J_c as the c cluster size. The statistical inference of the each cluster is then based on the low-dimensional time series analysis for Z_t. As shown by Park et al. (2009), the inference based on the estimates $\widehat{Z}_t^\top$ holds for "true" unobserved time series $Z_t^\top$, as the difference between $Z_t^\top$ and $\widehat{Z}_t^\top$ is asymptotically negligible.

2.3.3 General Linear Model and Testing Procedure

In practice, the analysis of BOLD fMRI data is conducted using voxelwise general linear model (GLM), see, e.g, Friston et al. (1994) and Worsley et al. (2002), where the magnetic resonance signal at voxel j is modeled by:

$$Y_j = \widetilde{X}\beta_j + e_j, \tag{8}$$

where $\widetilde{X}$ denotes the $T \times p$ design matrix, β_j is the $p \times 1$ vector of regression coefficients and e_j is a (often serially correlated) measurement error. The matrix $\widetilde{X}$ is constructed as a convolution of hemodynamic response function (HRF) $h(t)$ and the stimulus time signal and might also incorporate additional elements (i.e., temporal derivatives) when required by a specific experiment setup. It is common practice to model the HRF by a difference of two gamma functions, i.e.,

$$h(t) = (\frac{t}{5.4})^6 \exp\{-(t-5.4)/0.9)\} - 0.35(\frac{t}{10.8})^{12} \exp\{-(t-10.8)/0.9\}\,,$$

see, e.g., Worsley et al. (2002). Inference focuses on the estimates $\widehat{\beta}_j$ and the hypothesis $H_0 : \beta_j = 0$ is tested voxelwise (first-level analysis). $\widehat{\beta}_j$ being significantly different from 0 is interpreted as activation at the voxel j. Group analysis is usually done in the mixed-effects framework, where the activation pattern for i subject at j voxel $\widehat{\beta}^i_j$ serves as an input for the model (higher-level analysis). This standard technique implemented in FSL's FLAME (FMRIB's local analysis of mixed effects) is used here to test whether regression coefficients are significant and activation can be reported at the group level. The region of interest is reported to be significantly activated for clusters reaching uncorrected threshold of Z-score > 3.09 and consisting of at least 20 neighboring voxels. For more details we refer here to the technical reports of the FMRIB Analysis Group, see, e.g., Beckmann et al. (2003) and Beckmann and Smith (2004).

2.3.4 Cluster, Estimation, Activation and Decision (CEAD) Method

The resulting cluster representation by $\widehat{Z}_t^\top$ serves as the unit of analysis for the relevant signals related to the ID tasks and decisions. Profiting from higher signal-to-noise ratio present on the group level (Heller et al., 2006) clusters are tested for activation. For analysis of all participated subjects $i = 1, \ldots, I$, our multivariate scheme may be summarized in the following steps:

1. **C**luster-step: for each subject i construct the brain parcellation into C groups using spectral clustering NCUT algorithm.

2. **E**stimation-step: given the subject-specific clustering results, for subject i take the c cluster and fit the DSFM, given in (6). Repeat this estimation procedure for all clusters $c = 1 \ldots, C$ and all subjects $i = 1, \ldots, I$. The DSFM approach is thus applied $C \times I$ times separately.

3. **A**ctivation-step: representing (i, c), $i = 1, \ldots, I$, $c = 1 \ldots, C$ cluster dynamics by low-dimensional representation $\widehat{Z}_t^{(i,c)}$ test the time series activation in the GLM

framework. Select the activated clusters that are related to neural processes underlying (risky) investment decisions.

4. **D**ecision-step: investigate the activated factor loadings $\widehat{Z}_t^{(i,c)}$. Is the subjects investment behavior represented in any of the activated clusters? Is there any relation between the risk attitude and the low-dimensional time series?

2.4 Simulation Study

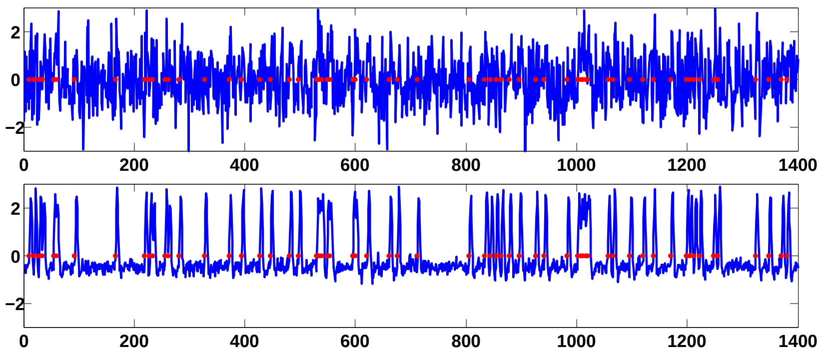

Figure 1: Setup (a): the simulated $(1,1,1)$ voxel $Y_{t,1}$ (top) and the estimated $\widehat{Z}_t$ (bottom) plotted against time (each 2 seconds); red dots denote stimulus; $\mathrm{Corr}_t(\widehat{Z}_t, \text{stimulus}) = 0.98$.

This part of our study is designed to investigate the performance of the proposed method in a simulation study. Our approach is evaluated against the benchmark, voxelwise GLM and the averaging technique introduced by Heller et al. (2006) (in each cluster take average over voxels and test for activation). We simulated data at one, exemplary cluster on the $6 \times 7 \times 6$ grid that mimics the average cluster obtained in our empirical analysis: $Y_t = Z_t^\top m(X) + \varepsilon_t$, where Y_t is a $6 \times 7 \times 6 \times 1400$ BOLD signal, $m(X) = m(x, y, z) = \|(x, y, z) - (6, 8, 6)\|$ is a smooth spatial structure, Z_t is a (perfect) stimulus time series (HRF $\times 64$, see Figure 10) and ε_t is noise. The (single) factor $m(\cdot)$ is a smooth, non-linear function that decreases in the direction of the point (6,8,6), that is not present on the grid, thus $m(\cdot) > 0$. The Z_t is the simplest design matrix (here 1×1400) from GLM setup and in this case stands for all stimuli corresponding to the correlated portfolio from our experiment. Therefore, we assume that only one true neural process is present in

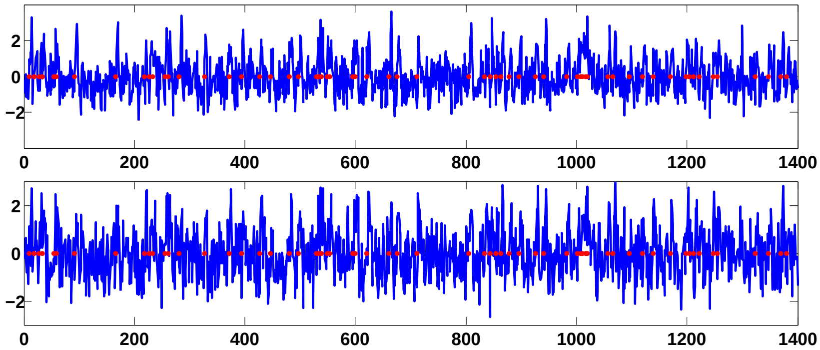

Figure 2: Setup (b): the simulated $(1, 1, 1)$ voxel $Y_{t,1}$ (top) and the estimated $\widehat{Z}_t$ (bottom) plotted against time (each 2 seconds); red dots denote stimulus; $\text{Corr}_t(\widehat{Z}_t, \text{stimulus}) = 0.60$.

this cluster. We investigate two possible cases for ε_t $(6 \times 7 \times 6 \times 1400)$: (a) ε_t is i.i.d. Gaussian and (b) ε_t is spatially correlated Gaussian; $\mu = 0$ and $\sigma = 1$. The spatially correlated noise time series $\varepsilon_{sc,t}$ is derived (independently at each t, $t = 1, \dots, 1400$) as a convolution of i.i.d. Gaussian noise from (a) with a spatial Gaussian kernel (FWHM 8 mm) and depicted in Figure 11. Examples of simulated BOLD signals are shown in Figures 1 and 2. The performance for all three techniques: DSFM with $L = 1$, GLM (pre-smoothed with FWHM 8 mm) and averaging over voxel in the cluster (with and without pre-smoothing) for the setup (a) is remarkably good and all statistics are higher than 100. The (b) study is summarized in Table 1. Firstly, all investigated techniques discover a significant activation and yield similar results. Secondly, the maximum Z-score in the GLM approach is the highest test statistics in all cases. When the Z-scores are averaged over all voxels, the DSFM approach yield the best result. Moreover, the simple averaging approach is outperformed by the DSFM. We conclude, that DSFM might serve as an interesting alternative to the benchmark GLM method, especially if the analysis goes beyond an identification of activation patterns (i.e., higher moments, time series analysis of voxels in a neighborhood).

	GLM	DSFM	Average(s)	Average
max Z-score	30.54	27.96	27.14	27.48
mean Z-score	26.34	27.96	27.14	27.48

Table 1: Test statistics Z-scores derived in simulation setup (b) for GLM, DSFM, averaging and averaging for smoothed (FHWM 8mm) data denoted by Average(s).

2.5 Behavioral Modeling

The subject specific risk attitudes can be directly derived from subject responses to ID tasks. Following Markowitz (1952); Caraco (1981) we apply the benchmark - mean-variance model to reflect the subjects decision making process:

$$V_i(x) = \overline{x} - \phi_i S(x), \tag{9}$$

where $V_i(x)$ is the *value* a subject i assigns to an investment x, $\overline{x}$ is an empirical mean and represents the *expected return*, $S(x)$ stands for a standard deviation and represents the subject's *risk*, and ϕ_i is the individual risk weight: risk attitude. Therefore, in line with the portfolio theory introduced by Markowitz (1952), we follow the common mean-variance approach.

The risk attitude can be estimated based on subject responses (risky choice vs. sure, 5% return) by the logistic model:

$$\mathsf{P}\left\{\text{risky choice}|x\right\} \quad = \quad \frac{1}{1+\exp\left\{\overline{x}-\phi S(x)-5\right\}}. \tag{10}$$

Negative values of $\widehat{\phi}_i$ indicate a risk seeking behavior, $\widehat{\phi}_i \approx 0$ relates to risk-neutrality and $\widehat{\phi}_i > 0$ to risk aversion. The estimated risk attitudes are shown in Figure 3 and additional analysis in Figures 12 and 13. For simplicity of presentation, in the subsequent part of the analysis we show data for two most extreme subjects: 19-th, risk-seeking: risk weight$=-0.0699$ and 1-st, risk-averse: risk weight$=1.092$.

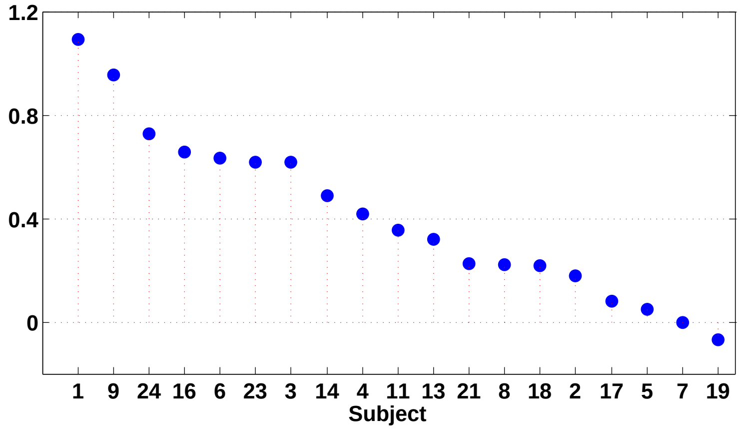

Figure 3: Risk attitudes of 19 subjects (indexed on x-axis) derived by the (10).

3 Results

Choice of the model parameters is described and the clustering results together with the estimated factor loadings are presented. This 2-step dimension reduction technique simplifies the brain dynamics into $C-$dimensional time series. The activated clusters are selected in the Activation-step and the subjects' risk aversion is modeled and predicted based only on the fMRI data.

3.1 Model Parameters

Selection of the number of clusters plays of course a role in our analysis. Choosing only few regions of interest (ROIs) (i.e., 50 parellations) leads to over-generalized and condensed regions that are anatomically distinctive, see, e.g., Craddock et al. (2012). Increasing the division into 200 clusters is reflecting the anatomical brain atlases (Talairach and Tournoux, 1988; Desikan et al., 2006) and an approach based on the brain identified atlas zones is often used. When a more precise parcellation is called for, practitioners then select 1000 clusters as discussed by Craddock et al. (2012). Our study aims to find activated brain regions related to the investment decisions, where the possible HRF may be subtle. Moreover, a successful implementation of the dynamic semiparametric factor model and conducted testing procedure requires highly accurate and homogenous inputs, we thus select $C = 1000$ clusters and ensure thereby the high accuracy of the representation. In the next step each (homogenous) cluster is represented by the DSFM technique with 1 dynamic factor, $L = 1$ for all cluster $c = 1, \dots, 1000$. Inclusion of higher number, though yielding a better fit, does not allow for a simple interpretation.

The parcellation technique is based on (1) as a proximity measure. In order to check stability of (1) over the entire experiment we conduct a moving window exercise. Figure 14 shows the correlation between 3 neighboring voxels derived by a rolling window exercise (for past $250 \approx 8$ min and $500 \approx 17$ min). One observes a stable, stationary behavior over time which stands in favor of our modelling setup.

3.2 Clustering Results

Clustering results are illustrated in Figure 4. The subject-specific parcellation, though computationally extensive, addresses inter-subject functional variability. Therefore, we derive spatially coherent regions of homogenous functional connectivity, that are present at a voxel scale. The clusters are contiguous sets of neighboring voxels and a distinction between network nodes and large-scale network of nodes is ensured, see Smith et al. (2009). The neuroscientific interpretability is preserved and further elaborated on in the modelling and testing part of our study. An average cluster is of a size 207 voxels, which might be compared to a $6 \times 6 \times 6 = 216$ (12 mm) cube. The smallest cluster is a singleton and the largest consist of 353 voxels. Clusters have a data-driven shape and vary with respect to the size and spatial structure as shown in Figure 15.

3.3 Factor Loadings $\widehat{Z}_t$

The clustering spatial maps serve as a basis for further exploratory analysis. The information carried in time evolution of the derived clusters is extracted by the DSFM technique.

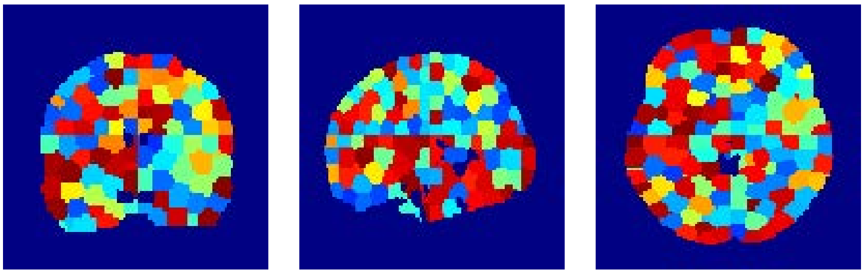

Figure 4: Illustration of the clustering results for subject 1 derived by the NCUT algorithm, $C = 1000$. The parcellation is represented as an orthogonal view and color-coding is arbitrarily used to capture the clusters' boundaries.

More precisely, all voxels belonging to cluster c of subject i: $Y^i_{c,1}, \dots, Y^i_{c,J^i_c}$, where J^i_c is the size of c cluster for subject i, are jointly modeled by (6). For simplicity of representation and as a natural consequence of cluster (homogenous) construction we employ the DSFM with $L = 1$. Thus, each cluster's dynamics are captured by the univariate time series $\widehat{Z}^{i,c}_t$, $i = 1, \dots, I$; $c = 1, \dots, 1000$, and the complete brain representation consist of 1000 processes. The derived brain model significantly simplifies the complexity of the data, while ensuring the interpretability and a good quality fit. For a demonstration two extreme subjects: 1 (with the smallest risk attitude) and 19 (with the largest risk attitude) are selected, see Figure 3. Figure 5 shows the estimated $\widehat{Z}^1_t$ and $\widehat{Z}^{19}_t$ for anterior insula (aINS; left and right) and dorsomedial prefrontal cortex (DMPFC) clusters. All factor loadings exhibits stationary behavior, high persitency and a high fluctuation around their mean value (see Figure 16 and Table 3), which may be related to the underlying investment decision stimulus.

3.4 Activation Results $\widehat{Z}_t$

The derived low-dimensional representation of each cluster $\widehat{Z}_t$ serves as a principal unit of this study and is tested for activation. We compare our method with both, the standard voxelwise GLM technique and the approach proposed by Heller et al. (2006) (average over voxels and use it as a cluster temporal representation). Four separate analyses were conducted (single, correlated and uncorrelated, jointly all types of portfolio). For each

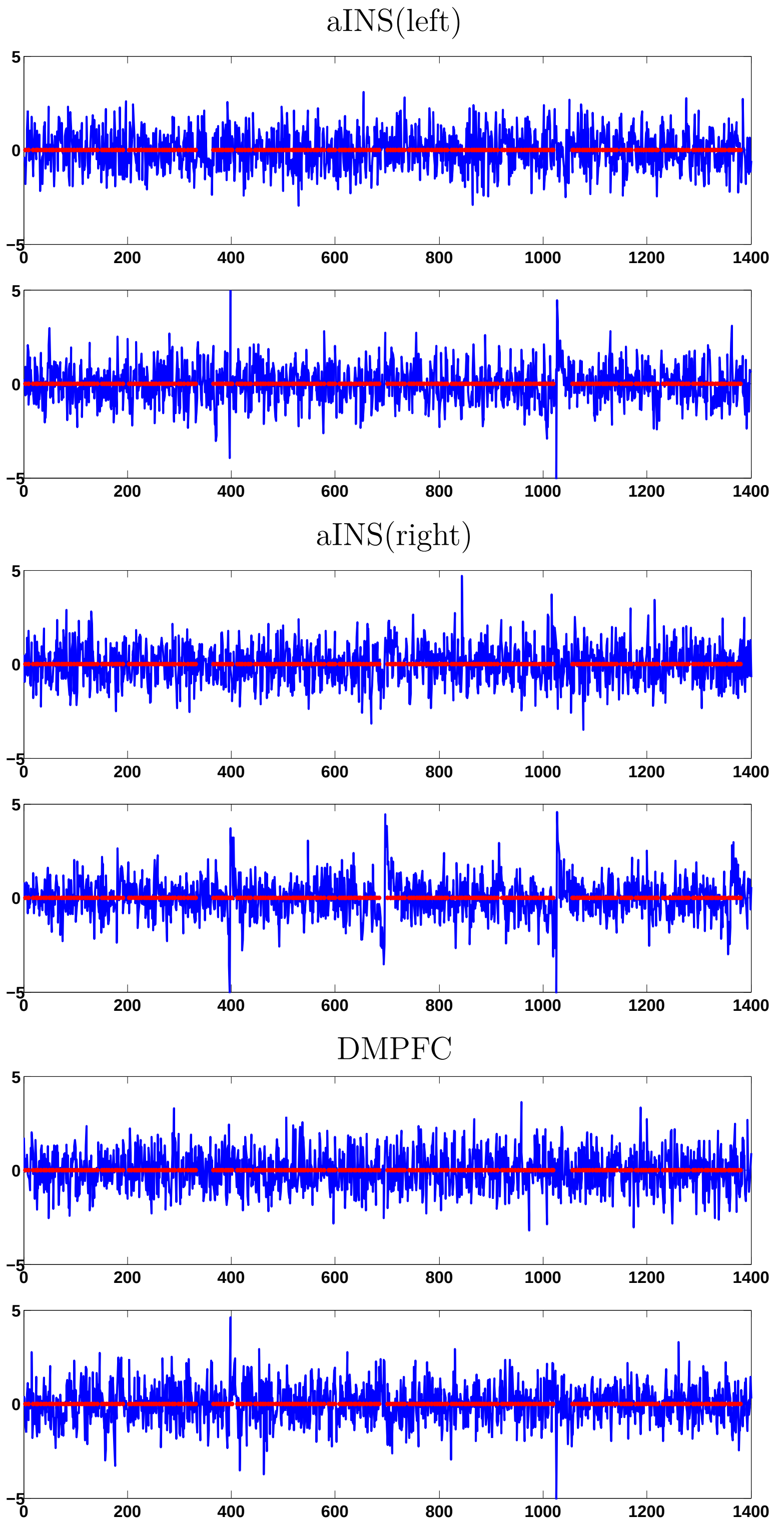

Figure 5: Factors loadings $\widehat{Z}_t$ for clusters aINS(left), aINS(right) and DMPFC (upper, middle lower panel) for risk averse subject 1 (top) and weakly risk seeking subject 19 (bottom) plotted against time (each 2 seconds). Red points correspond to the time points of stimuli.

type of investment we reported the same activation pattern, thus only the joint analysis (all portfolios) is reported here.

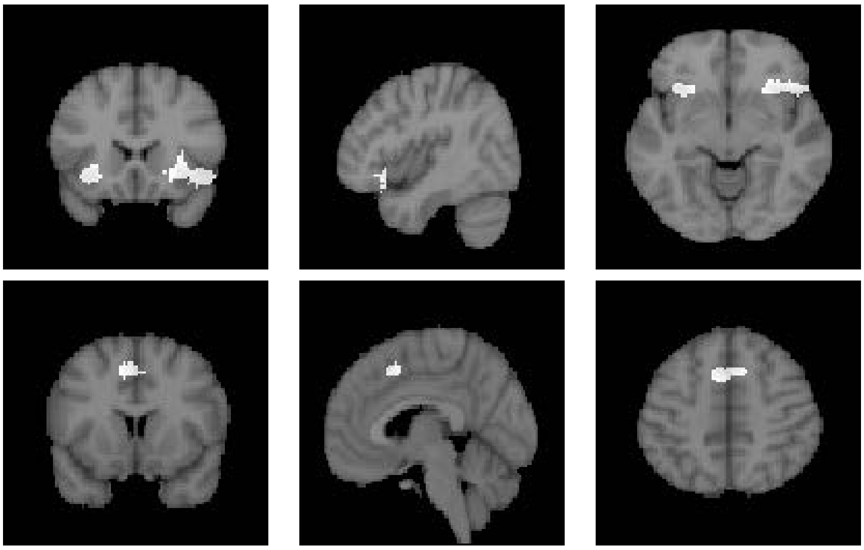

Figure 6: Results of the higher-level analysis (mixed-effects model) associated with decision making; Z-scores$>$ 3.09. Upper panel: the bilateral aINS, lower panel: DMPFC.

Figure 6 presents significant brain correlates of the ID task: aINS and DMPFC associated with decision making. These activation results are in line with findings by Mohr, Biele, Krugel, Li and Heekeren (2010); Mohr, Biele and Heekeren (2010) and contribute to the neural foundations of risk-return model. Altogether 9 activated clusters were detected which survived statistical tresholding at Z-scores$>$ 3.09 and had a cluster size of at least 20 voxels. Besides aINS and DMPFC factors corresponding to decision making, we identified other brain regions previously associated with visual perception and motoric responses. These factors are most likely not connected to the decision making process but confirm the activity of regions which were necessary to give the answer by pushing the button. Average reactions to the ID stimuli over all 19 subjects are depicted in Figure 7. Reported maximum Z-scores for aINS and DMPFC are shown in Table 4. One observes that all approaches yield very similar results, though the highest maximum Z-score is achieved by the GLM technique for all 3 ROIs. Secondly, the DSFM outperforms the simple averaging over voxels. The non-parametric estimation pays off in terms of the quality of the representation.

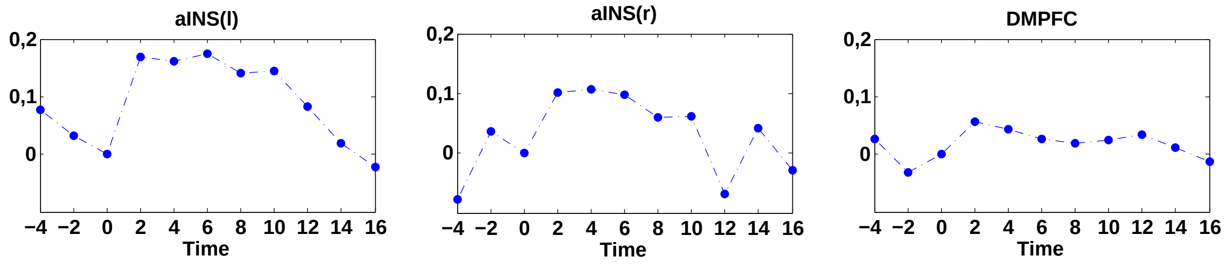

Figure 7: Average reaction to the ID stimulus over all 19 subjects for bilateral aINS and DMPFC regions plotted against time (from -4 seconds before the stimuli up to 16 seconds afterwards).

4 Risk Attitude \ Stimulus Response

The key goal in neuroeconomics is to "(...) ground economic theory in detailed neural mechanisms which are expressed mathematically and make behavioral predictions." as Camerer (2007, 2013) states. Motivated by that, we investigated a connection between the neural processes underlying decision making and risk perception. Without prior knowledge of the subjects' answers, based only on the activated cluster dynamics, represented by $\widehat{Z}_t$ a simple model is proposed to predict the risk attitude ϕ_i. As described in section (3.4) three activated (see Table 4) clusters are associated with decision making under risk. Therefore only cluster dynamics of bilateral aINS and DMPFC are considered here as regressors for the risk attitude ϕ_i. These loadings (brain regions) respond to the stimulus and thus mimic neural processes present in a whole cluster during investment decisions under risk in our study. The hemodynamic response function usually peaks around 6 seconds after the stimulus. Therefore, we focus on an average reaction to r, $r = 1, \ldots, 256$, stimulus for the i-th subject: $\Delta\widehat{Z}^i_r = \frac{1}{4}\sum_{\tau=1}^{4} \widehat{Z}^i_{r+\tau} - \widehat{Z}^i_r$. $\Delta\widehat{Z}^i_r$ covers a period up to 8 seconds afterwards and ensures that the HRF maximum is captured. An average reaction to all stimuli (entire experiment) for a single cluster is defined as $\overline{\Delta}\widehat{Z}^i = \frac{1}{256}\sum_{r=1}^{256} \Delta\widehat{Z}^i_r$. Our model-free methodology closely follows the statistics proposed by van Bömmel et al. (2013); Brown et al. (2014).

Understanding which among the variables: $\overline{\Delta}\widehat{Z}_{aINS(l)}$, $\overline{\Delta}\widehat{Z}_{aINS(r)}$, $\overline{\Delta}\widehat{Z}_{DMPFC}$ are related to the ϕ and an exploration of the forms of these relationships is done via regression analysis. More precisely:

$$\phi_i = \alpha_0 + \alpha_1 \cdot \overline{\Delta}\widehat{Z}^i_{DMPFC} + \alpha_2 \cdot \overline{\Delta}\widehat{Z}^i_{aINS(l)} + \alpha_3 \cdot \overline{\Delta}\widehat{Z}^i_{aINS(r)} + \widetilde{\varepsilon}^i, \tag{11}$$

where α_0 is an intercept, $\alpha = (\alpha_1, \alpha_2, \alpha_3)^\top$ is a vector of regression coefficients and $\widetilde{\varepsilon}$ stands for the error term. In other words, (spatially constrained, local) information extracted from the BOLD signal serves as regressors for the subject's risk weights.

	Estimate	SE	t-statistic	p-value
α_0	0.097	0.115	0.861	0.403
$\overline{\Delta}\widehat{Z}_{DMPFC}$	0.851	0.526	1.619	0.126
$\overline{\Delta}\widehat{Z}_{aINS(r)}$	-1.506	0.550	-2.737	0.015
$\overline{\Delta}\widehat{Z}_{aINS(l)}$	-1.126	0.379	-2.967	0.001

Table 2: Risk attitude regressed on the average response for all 19 subjects; $R^2 = 0.47$, *adjusted* $R^2 = 0.36$.

Summary statistics of the model defined in (11) are reported in Table 2. Surprisingly, we report that the DMPFC factor, though significantly activated, does not carry explanatory power for risk preferences. This finding, among others, goes far beyond classical fMRI analysis done within the GLM framework and highlights the flexibility and advantages of our approach. Furthermore, the aINS, both left and right regions, are picked up by the model and reported p-values are remarkably smaller than 0.05. Overall, the explanatory power is satisfactory despite the simplicity of linear relation and the noisy nature of the studied panel data (for both, BOLD signal and risk weights). We obtain $R^2 = 0.47$ and *adjusted* $R^2 = 0.36$. The regression fit is depicted in Figure 8. Dropping out of the insignificant terms in (11) yields:

$$\phi_i = \alpha_2 \cdot \overline{\Delta}\widehat{Z}^i_{aINS(l)} + \alpha_3 \cdot \overline{\Delta}\widehat{Z}^i_{aINS(r)} + \widetilde{\varepsilon}^i. \tag{12}$$

The simplified model achieves $R^2 = 0.37$, *adjusted* $R^2 = 0.30$ and the p-values are 0.03 and 0.02 for $\overline{\Delta}\widehat{Z}_{aINS(r)}$ and $\overline{\Delta}\widehat{Z}_{aINS(l)}$, respectively. Figure 8 shows the regression fit. In

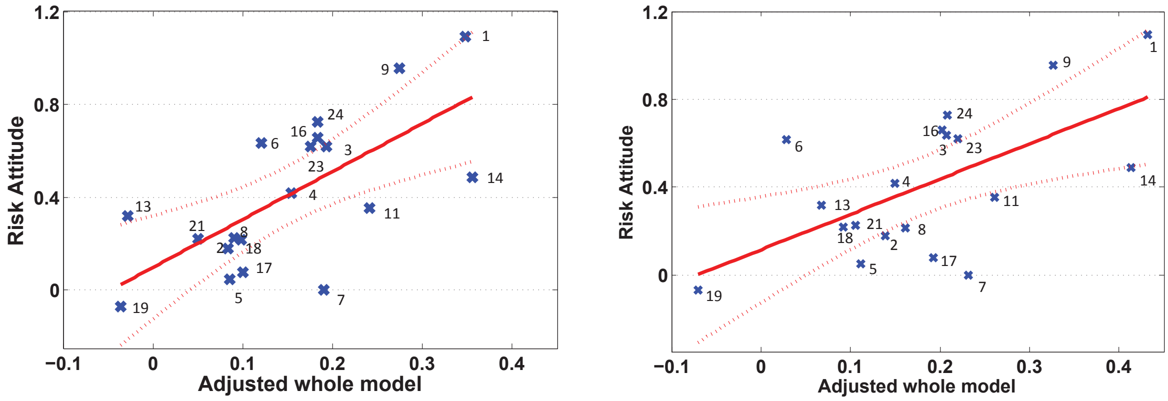

Figure 8: Added variable plot for models given in (11) left, (12) right panel, respectively. Horizontal axis denotes the (rescaled) best linear combination of regressors $\overline{\Delta}\widehat{Z}$ that fit ϕ.

this setup subject risk aversion depends only on the average reaction to the stimulus in the aINS regions. This setup, consisting only of activated (see Table 4) and significant BOLD cluster statistics is kept in the reminder of the analysis.

4.1 Risk Attitude Forecasting

The regression results presented in Table 2 indicate that the DMPFC factor is not significant and does not carry explanatory power for ϕ_i. Thus, the regression setup, stated in (12) is used to predict the subject risk attitude based only on the information extracted from BOLD signal in aINS. For each subject $i = 1, \dots, 19$ its information is excluded from the regression analysis and the model (12) is re-estimated. Plugging-in the neural low-dimensional representation: $\overline{\Delta}\widehat{Z}^i_{aINS(l)}$ and $\overline{\Delta}\widehat{Z}^i_{aINS(r)}$ to the new model predicts the risk weight ϕ_i and the out-of-sample performance is shown in Figure 9. Seven predicted risk attitudes, out of 19, lie out of 95% prediction confidence intervals and the absolute average forecasting error is 0.257. One could expect that the proposed statistics $\overline{\Delta}\widehat{Z}$ is not the best univariate projection of the hemodynamic response to the stimulus. To overcome some possible deviations in the HRF peak's location we apply the weighted average reaction to the stimulus denoted by a weighted average reaction: $\Delta_w \widehat{Z}^i_r = \sum_{\tau=1}^4 w_\tau(\widehat{Z}^i_{r+\tau} - \widehat{Z}^i_r)$, with $\sum_{\tau=1}^4 w_\tau = 1$. Thus, observations after stiumuls are weighted with unknown weights

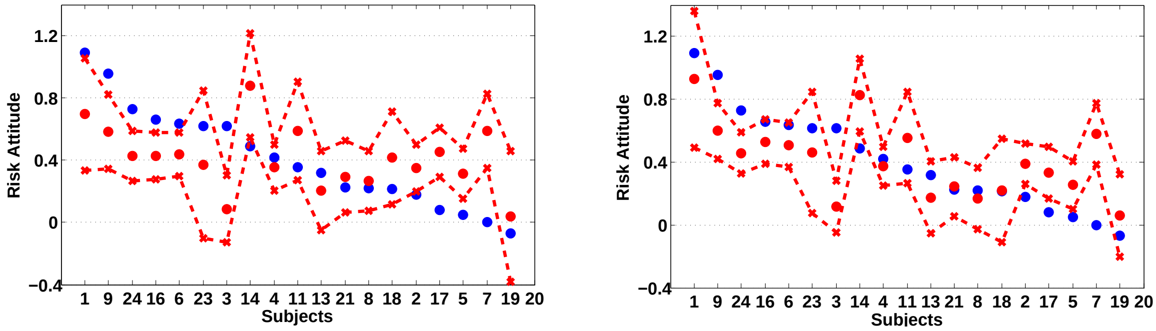

Figure 9: Predicted risk preferences by the model given in (11) for the average $\overline{\Delta}\widehat{Z}$ and the weighted average $\overline{\Delta}_w\widehat{Z}$: left, right panel, respectively. Information extracted from the aINS BOLD signal; $w = (0.38, 0.41, 0.16, 0.05)^\top$.

w_τ. The procedure introduced before is repeated for $\Delta_w\widehat{Z}^i = \frac{1}{256}\sum_{r=1}^{256}\Delta_w\widehat{Z}_r^i$ and the weights are found by minimizing the absolute average forecasting error. The optimal weights $w = (0.38, 0.41, 0.16, 0.05)^\top$ are derived by Monte Carlo simulation with 10000 iterations and the new absolute average prediction error is 0.202. The prediction fit is reported in Figure 9. In this setup the first 3 observations (up to 6 seconds after stimuli) exhibit a remarkably higher impact than the 4-th one.

The neural predictions of risk attitudes, though satisfactory, do not perfectly match risk weights derived from subjects' investment decisions. A plausible explanation from a statistical point of view would be the simplicity of linear relation, inhomogeneity of studied subjects and above all, the noisy nature of the data. Nevertheless, we are convinced, that the neural processes underlying investment decisions and corresponding risk preferences are a far more complex phenomenon and go beyond the aINS and DMPFC only. Our statistical methodology is constrained here by the experiment setup that, naturally, cannot capture all brain reactions and allows only to estimate a proxy of "true" risk preferences by risk-return model. Though the activation is reported by the benchmark testing procedure, we suspect additional brain regions to contribute to investment decisions (e.g., Mohr, Biele and Heekeren (2010)) not identified in this fMRI study. This goes beyond the scope of this paper and deserves further research.

5 Discussion

We have presented a novel method for analyzing fMRI data based on cluster units: CEAD. In the first step the clusters are derived via the NCUT algorithm as contiguous groups of voxels and there are no further constraints concerning the shape and spatial structure. This data-driven approach makes use of the correlation between neighboring voxels and therefore ensures a co-movement of the BOLD signals within cluster. This property of "anatomic" homogeneity pays off when temporal information carried by each cluster has to be extracted. Derived functional connectivity maps are a starting point of analysis. In the estimation-step the DSFM method is applied on each cluster and serves here as a dimension reduction technique. It serves as a filter of the noise and only extracts the common temporal information: the signal (i.e., joint reaction to the stimulus). This semi-parametric approach can handle various specifications of noise observed at the voxel level and yields favorable results in comparison to simple averaging over voxels (Heller et al., 2006). It is a model-free technique that derives complete spatiotemporal information from brain regions. In the activation-step, the extracted signal is further studied for experimental responses. Our local-dynamic representation yields similar results as traditional GLM analyses. The high accuracy of the model plays an important role when possible task-related effects are subtle and local. Our approach ensures a simplicity of neural interpretation and addresses the key limitations of the benchmark method GLM. In the decision step the CEAD method allows for any model-free analysis of spatiotemporal ROI's information.

We apply the CEAD methodology to study neural systems that underlie decision making under risk. In particular, investment decision is a complex process of valuation and comparison of possible choices with unknown outcomes. Risk attitude is a crucial metric that influences the subjective value of investment. In this paper we analyzed an fMRI experiment with 19 subjects. Each subject was scanned during multiple RPID tasks and a series of 1400 images of $91 \times 109 \times 91$ voxels are investigated here. Using our methodology we decomposed individual brains into sets of 1000 spatially disjoint factors and factor loadings $\widehat{Z}_t^{i,c}$, $i = 1, \ldots, 19$ and $c = 1, \ldots, 1000$. Derived spatiotemporal representation is subject-specific and possible variations in functional brain structure are addressed. Therefore we ensure high accuracy and interpretability of the results. Extracted $\widehat{Z}_t$ are tested for activation in the GLM (mixed-effects model) framework. For the studied population we detect significant activation at aINS and DMPFC regions as correlates for risk, already reported in Mohr, Biele and Heekeren (2010). Our approach yields similar results to the benchmark and is complimentary.

To deepen our understanding of changes in neural activity underlying risk preferences we conducted a model-free analysis. The focus is on those ROIs that show ID-related effects: aINS (left and right) and DMPFC (see Table 4) which have previously been associated with decision making. More precisely, we explore the relation between average reaction to the stimulus in subject-specific loadings $\widehat{Z}_t$ representing selected regions. Following Brown et al. (2014) we construct simple, model-free statistics that capture the peak of HRF: $\overline{\Delta}\widehat{Z}_{aINS(l)}$, $\overline{\Delta}\widehat{Z}_{aINS(r)}$, $\overline{\Delta}\widehat{Z}_{DMPFC}$ and explore their explanatory power on the risk attitude ϕ_i. The resulting regression model with brain dynamics as regressors achieves $R^2 = 0.47$. Changes in brain activity represented by $\overline{\Delta}\widehat{Z}_{DMPFC}$ did not carry informative power for risk attitude. Simultaneously, both aINS regions are picked up to be statistically significant and reported p-values are ≈ 0.01. We conclude that DMPFC, though activated by the risk of the investment, is not significantly correlated to risk attitudes. Dropping off all irrelevant terms and reestimating the regression model (12) yields $R^2 = 0.37$. This parsimonious and informative setup is used to predict the risk attitudes based only on fMRI information. The analysis is further refined adjusting for possible variation of hemodynamic response by adding the weights to the sequence of observations after stimulus.

We report, that neural predictions of risk attitudes, though satisfactory, do not mimic perfectly risk weights derived from subject investment decisions. One may claim that the applied mean-variance model does not reflect true risk attitudes adequately well and additional measures for subjective expected returns and perceived risk than mean and standard deviation should be introduced. Secondly, the risk preferences and neural responses identified in this study may not cover all the effects and brain reactions. Risk attitude is far more complex and may not be only localized in aINS. Therefore we plan to apply our methodology to a wide spectrum of similar studies for further investigations.

6 Appendix

6.1 Simulation Study

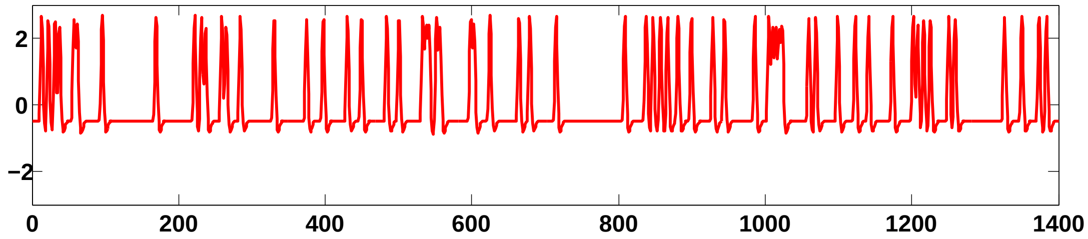

Figure 10: Stimulus time series derived as a convolution of double Gamma hemodynamic response function and uncorrelated portfolio stimulus $\times 64$ plotted against time (each 2 seconds).

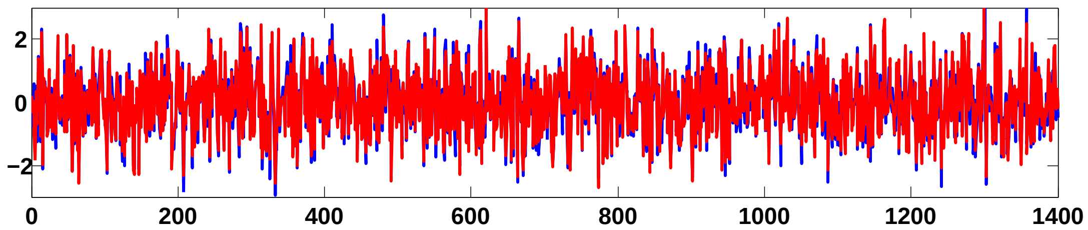

Figure 11: Simulated spatially correlated Gaussian noise for 2 vertical neighbor voxels (red and blue) plotted against time (each 2 seconds); $\mathrm{Corr}_t(\varepsilon_{t,1}, \varepsilon_{t,2}) = 0.97$.

6.2 Clustering and Sensitivity Analysis

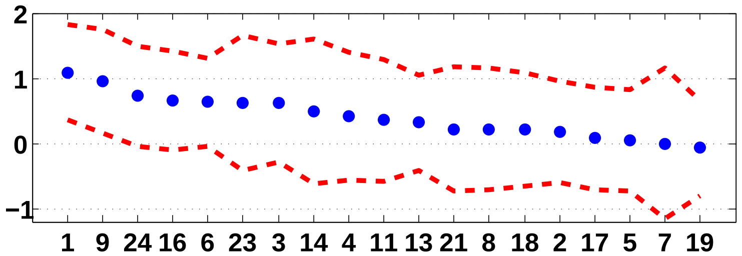

Figure 12: Sensitivity analysis of the risk attitude ϕ: estimates $\widehat{\phi}_i, i = 1, \ldots, 19$ with 95% confidence intervals.

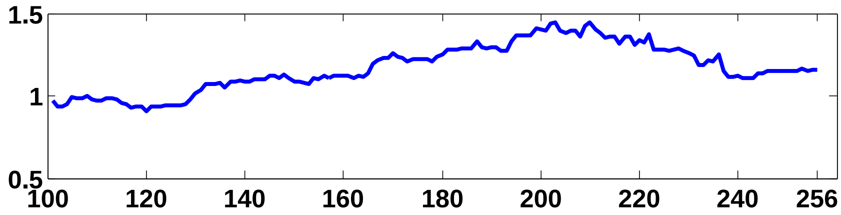

Figure 13: The derived risk attitude of subject 1 in a rolling window exercise ($\widehat{\phi}_i$ estimated from past 100 ID answers).

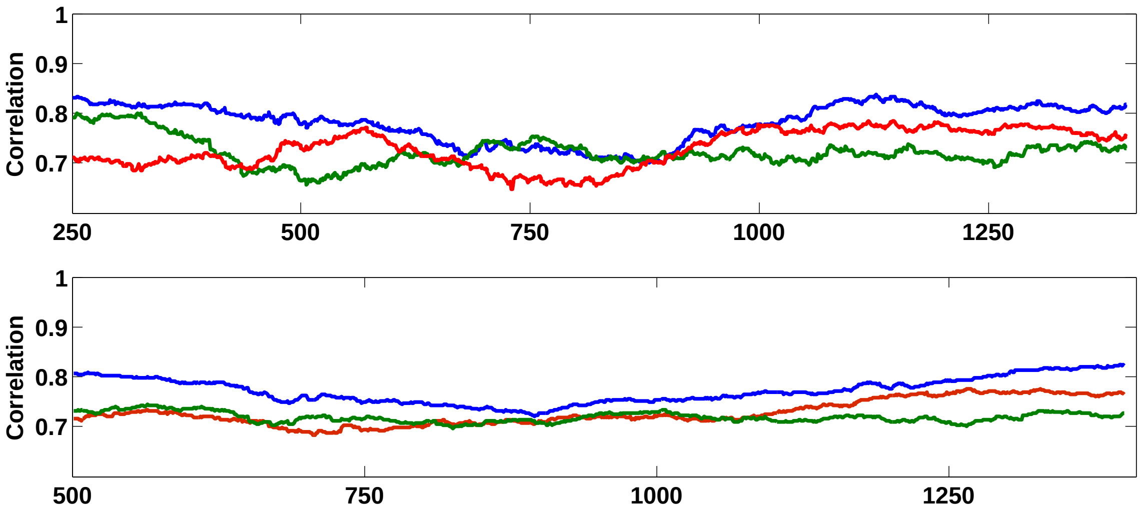

Figure 14: Time series of the correlation coefficient derived by the rolling window (250 top, 500 bottom) for the center voxel and: horizontal, vertical diagonal neighboring voxel for aINS(right) of subject 1.

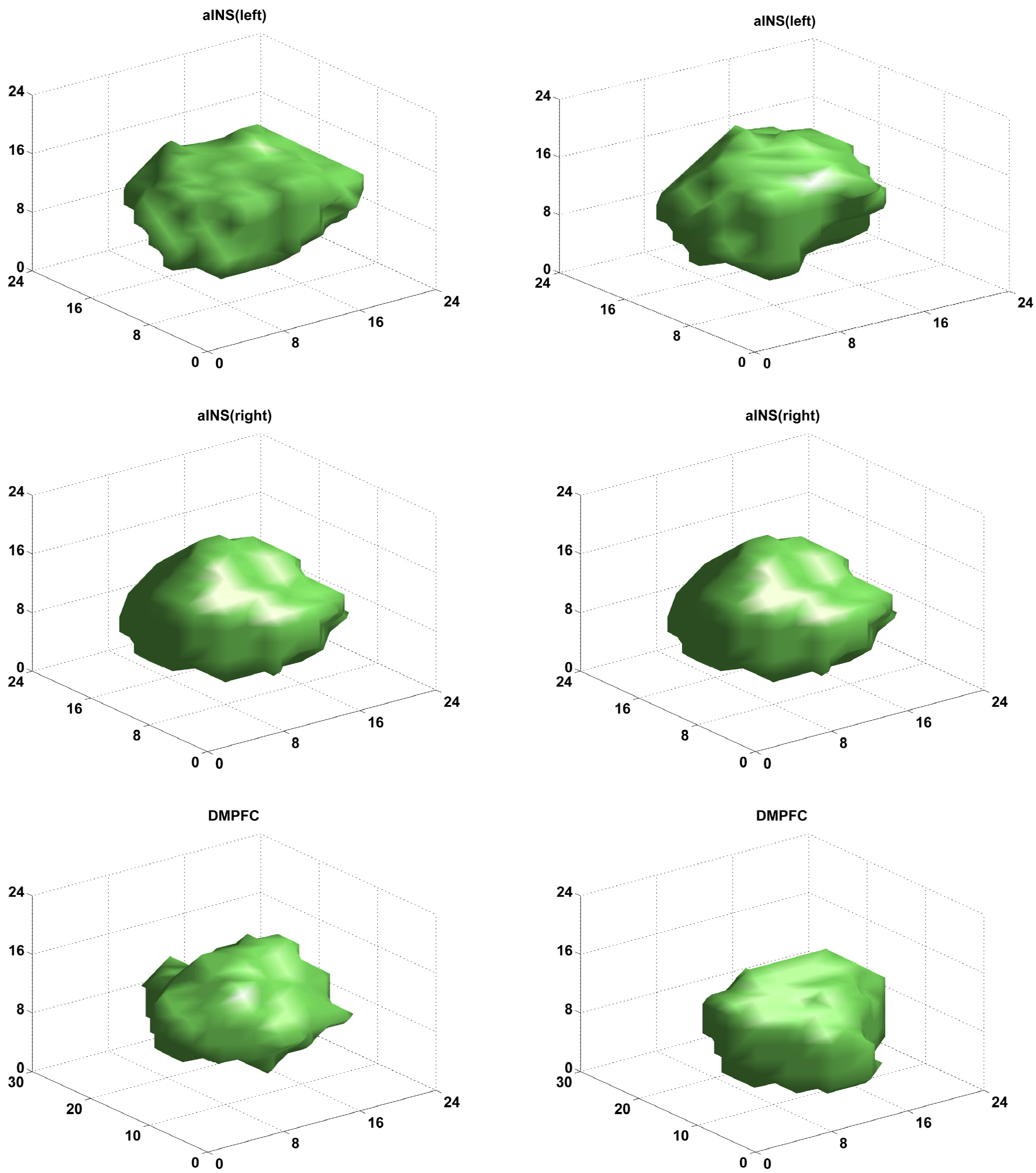

Figure 15: Contour plots of derived aINS(left), aINS(right) and DMPFC (upper, middle lower panel) clusters for subjects 1 (left) and 19 (right), respectively; derived by the NCUT algorithm with $C = 1000$. x-, y- z-axis denote the $3D$ space given in millimeters.

6.3 Factor Loadings

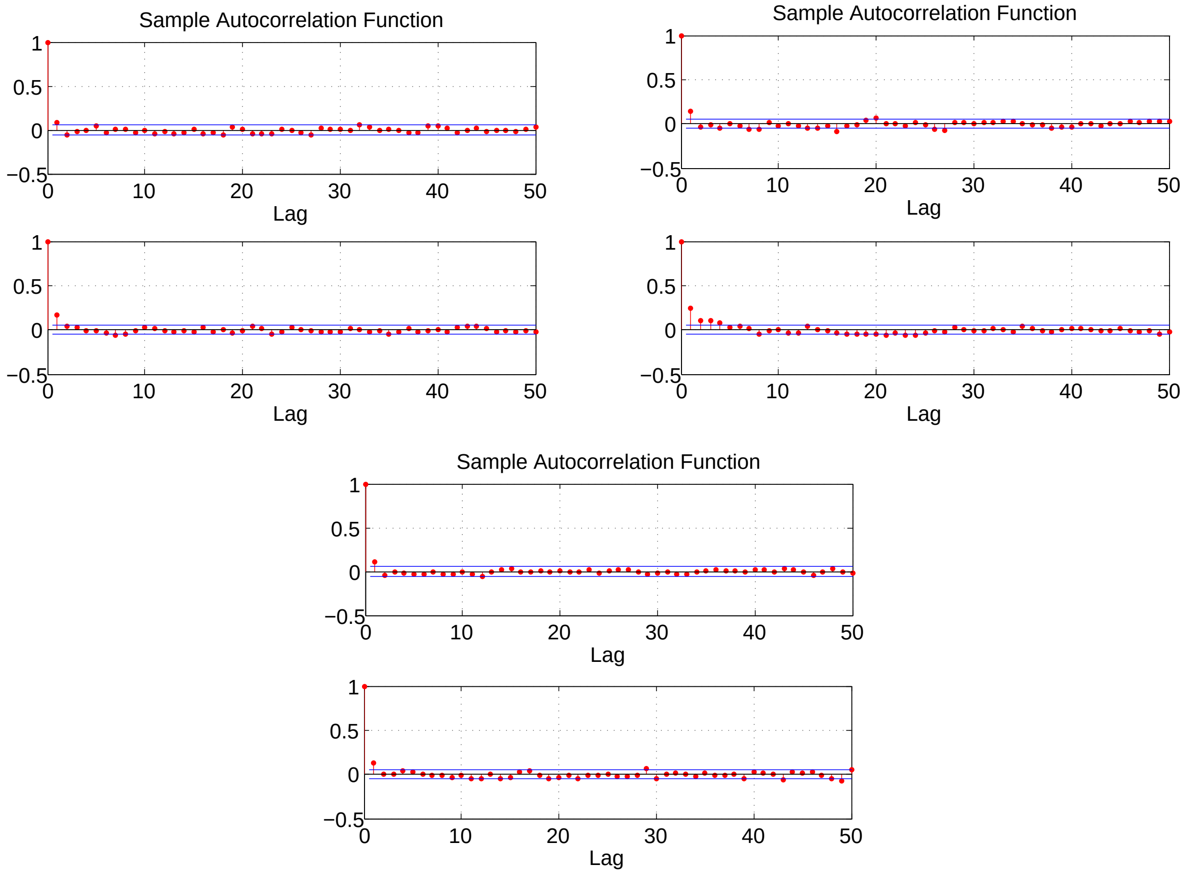

Figure 16: Sample autocorrelation function of aINS(left), aINS(right) and DMPFC $\widehat{Z}_t$ (top left, top right, bottom panel, respectively) for subjects 1 (top) and 19 (bottom), respectively.

	aINS(l)	aINS(r)	DMPFC	aINS(l)	aINS(r)	DMPFC
KPSS	0.035	0.063	0.038	0.044	0.051	0.044
ADF	−0.128	−0.137	−0.110	−0.185	−0.207	−0.159

Table 3: KPSS, ADF test statistics for estimated factor loadings aINS(left), aINS(right) and DMPFC $\widehat{Z}_t$; subject 1 (left panel), subject 19 (right panel) (KPSS: H_0: weak stationarity, critical values at 0.10, 0.05, 0.01 are 0.119, 0.146 and 0.216; ADF: H_0: unit root, critical values at 0.01, 0.05, 0.10 are −1.61, −1.94 and −2.58).

	DSFM	Average	GLM
aINS(l)	$(-34, 18, -8)$ 4.13 3×10^{-4}	$(-36, 18, -8)$ 4.08 4×10^{-4}	$(-32, 22, -12)$ 4.58 3×10^{-3}
aINS(r)	$(34, 24, -4)$ 4.39 6×10^{-6}	$(36, 18, -6)$ 4.21 6×10^{-7}	$(40, 22, -16)$ 5.24 3×10^{-7}
DMPFC	$(6, 24, 42)$ 4.43 2×10^{-9}	$(4, 24, 42)$ 3.88 1×10^{-8}	$(4, 24, 24)$ 4.56 3×10^{-7}

Table 4: The position of the cluster local maximum, denoted in the MNI (Montreal Neurological Institute) standard at 2mm resolution, corresponding Z-score (middle) and p-value (bottom) of activated "risk" clusters during the ID stimuli. Average stands for a mean value over voxels in each cluster (results of the NCUT parcellation with $C = 1000$). Analysis done in the FSL (FEAT/FLAME) software.

References

Beckmann, C. F., Jenkinson, M. and Smith, S. M. (2003). General multilevel linear modeling for group analysis in FMRI, *NeuroImage* **20**(2): 1052–1063. DOI: 10.1016/S1053-8119(03)00435-X.

Beckmann, C. F. and Smith, S. M. (2004). Probabilistic independent component analysis for functional magnetic resonance imaging, *IEEE Transactions on Medical Imaging* **23**(2): 137–152. DOI: 10.1109/TMI.2003.822821.

Beckmann, C. F. and Smith, S. M. (2005). Tensorial extensions of independent component analysis for multisubject FMRI analysis, *NeuroImage* **25**(1): 294–311. DOI: 10.1016/j.neuroimage.2004.10.043.

Bernoulli, D. (1738). Specimen Theoriae Novae de Mensura Sortis, *Papers of the Imperial Academy of Sciences in Petersburg* **5**: 172–192.

Brown, D. A., Lazar, N. A., Datta, G. S., Jang, W. and McDowell, J. E. (2014). Incorporating spatial dependence into Bayesian multiple testing of statistical parametric maps in functional neuroimaging, *NeuroImage* **84**(1): 97–112. DOI: 10.1016/j.neuroimage.2013.08.024.

Camerer, C. F. (2007). Neuroeconomics: Using Neuroscience to Make Economic Predictions, *The Economic Journal* **117**(519): C26–C42. DOI: 10.1111/j.1468-0297.2007.02033.x.

Camerer, C. F. (2013). Goals, methods, and progress in neuroeconomics, *Annual Review of Economics* **5**(1): 425–455. DOI: 10.1146/annurev-economics-082012-123040.

Caraco, T. (1981). Energy budgets, risk and foraging preferences in dark-eyed juncos (Junco hyemalis), *Behavioral Ecology and Sociobiology* **8**(3): 213–217. DOI: 10.1007/BF00299833.

Craddock, R. C., James, G. A., Holtzheimer, P. E., Hu, X. P. and Mayberg, H. S. (2012).

A whole brain fMRI atlas generated via spatially constrained spectral clustering, *Human Brain Mapping* **33**(8): 1914–1928. DOI: 10.1002/hbm.21333.

Desikan, R. S., Segonne, F., Fischl, B., Quinn, B. R., Dickerson, B. C., Blacker, D., Buckner, R. L., Dale, A. M., Maguire, R. P., Hyman, B. T., Albert, S. A. and Killiany, R. J. (2006). An automated labeling system for subdividing the human cerebral cortex on MRI scans into gyral based regions of interest, *NeuroImage* **31**(3): 968–980. DOI: 10.1016/j.neuroimage.2006.01.021.

Friston, K. J., Holmes, A. P., Worsley, K. J., Poline, J.-P., Frith, C. D. and Frackowiak, R. S. J. (1994). Statistical parametric maps in functional imaging: A general linear approach, *Human Brain Mapping* **2**(4): 189–210. DOI: 10.1002/hbm.460020402.

Garrett, D. D., Samanez-Larkin, G. R., MacDonald, S. W., Lindenberger, U., McIntosh, A. R. and Grady, C. L. (2013). Moment-to-moment brain signal variability: A next frontier in human brain mapping?, *Neuroscience and Biobehavioral Reviews* **37**(4): 610 – 624. DOI: 10.1016/j.neubiorev.2013.02.015.

Glimcher, P. W. and Fehr, E. (2013). *Neuroeconomics: Decision making and the brain. Second Edition*, Academic Press. ISBN: 9780124160088.

Heekeren, H. R., Marrett, S. and Ungerleider, L. G. (2008). The neural systems that mediate human perceptual decision making, *Nature Reviews Neuroscience* **9**(6): 467–479. DOI: 10.1038/nrn2374.

Heller, R., Stanley, D., Yekutieli, D., Rubin, N. and Benjamini, Y. (2006). Cluster-based analysis of FMRI data, *NeuroImage* **33**(2): 599–608. DOI: 10.1016/j.neuroimage.2006.04.233.

Kable, J. W. and Glimcher, P. W. (2007). The neural correlates of subjective value during intertemporal choice, *Nature Reviews Neuroscience* **10**: 1625–1633.

Kahneman, D. and Tversky, A. (1979). Prospect Theory: An Analysis of Decisison under Risk, *Econometrica* **47**(2): 263–292. DOI: 10.2307/1914185.

Kamvar, S. D., Klein, D. and Manning, C. D. (2003). Spectral Learning, *Proceedings of the 18th International Joint Conference on Artificial Intelligence*, IJCAI'03, Morgan Kaufmann Publishers Inc., San Francisco: 561–566. ISBN: 9780127056616.

Logothetis, N. K. (2008). What we can do and what we cannot do with fMRI, *Nature* **453**(7197): 869–878. DOI: 10.1038/nature06976.

Luxburg, U. (2007). A tutorial on spectral clustering, *Statistics and Computing* **17**(4): 395–416. DOI: 10.1007/s11222-007-9033-z.

Markowitz, H. (1952). Portfolio Selection, *Journal of Finance* **7**(1): 77–91. DOI: 10.1111/j.1540-6261.1952.tb01525.x.

Mohr, P., Biele, G. and Heekeren, H. (2010). Neural Processing of Risk, *The Journal of Neuroscience* **30(19)**: 6613–6619. DOI: 10.1523/JNEUROSCI.0003-10.2010.

Mohr, P. N. C., Biele, G., Krugel, L. K., Li, S.-C. and Heekeren, H. R. (2010). Neural foundations of risk-return trade-off in investment decisions, *NeuroImage* **49**(3): 2556–2563. DOI: 10.1016/j.neuroimage.2009.10.060.

Mohr, P. N. C. and Nagel, I. E. (2010). Variability in Brain Activity as an Individual Difference Measure in Neuroscience?, *The Journal of Neuroscience* **30**(23): 7755–7757. DOI: 10.1523/JNEUROSCI.1560-10.2010.

Park, B. U., Mammen, E., Härdle, W. K. and Borak, S. (2009). Time Series Modelling With Semiparametric Factor Dynamics, *Journal of the American Statistical Association* **104**(485): 284–298. DOI: 10.1198/jasa.2009.0105.

Ruff, C. C. and Huettel, S. A. (2013). Neuroeconomics: Decision making and the brain. second edition, Academic Press, chapter Experimental methods in cognitive neuroscience. ISBN: 9780124160088.

Shen, X., Papademetris, X. and Constable, R. T. (2010). Graph-theory based parcellation of functional subunits in the brain from resting-state fMRI data, *NeuroImage* **50**(3): 1027–1035. DOI: 10.1016/j.neuroimage.2009.12.119.

Shi, J. and Malik, J. (2000). Normalized cuts and image segmentation, *IEEE Transactions on Pattern Analysis and Machine Intelligence* **22**(8): 888–905. DOI: 10.1109/34.868688.

Smith, S. M., Fox, P. T., Miller, K. L., Glahn, D. C., Fox, P. M., Mackay, C. E., Filippini, N., Watkins, K. E., Toro, R., Laird, A. R. and Beckmann, C. F. (2009). Correspondence of the brain's functional architecture during activation and rest, *Proceedings of the National Academy of Sciences of the United States of America* **106**(31): 13040–13045. DOI: 10.1073/pnas.0905267106.

Talairach, J. and Tournoux, P. (1988). *Co-Planar Stereotaxic Atlas of the Human Brain: 3-D Proportional System: An Approach to Cerebral Imaging (Thieme Classics)*, Thieme, Stuttgart. ISBN: 9783137117018.

van Bömmel, A., Song, S., Majer, P., Mohr, P. N. C., Heekeren, H. R. and Härdle, W. K. (2013). Risk Patterns and Correlated Brain Activities. Multidimensional Statistical Analysis of fMRI Data in Economic Decision Making Study, *Psychometrika*. DOI: 10.1007/s11336-013-9352-2.

van den Heuvel, M., Mandl, R. and Hulshoff Pol, H. (2008). Normalized Cut Group Clustering of Resting-State fMRI Data, *PLoS One* **3**(4): e2001. DOI: 10.1371/journal.pone.0002001.

von Neumann, J. and Morgenstern, O. (1953). *Theory of Games and Economic Behavior*, Princeton University Press, Princeton. ISBN: 9781400829460.

Weber, E. U. and Milliman, R. A. (1997). Perceived Risk Attitudes: Relating Risk Perception to Risky Choice, *Management Science* **43**(2): 123–144. DOI: 10.1287/mnsc.43.2.123.

Worsley, K. J., Liao, C. H., Aston, J., Petre, V., Duncan, G. H., Morales, F. and Evans, A. C. (2002). A General Statistical Analysis for fMRI Data, *NeuroImage* **15**(1): 1–15. DOI: 10.1006/nimg.2001.0933.

Xu, Q., desJardins, M. and Wagstaff, K. (2005). Constrained Spectral Clustering under a Local Proximity Structure Assumption, *Proceedings of the 18th International Florida Artificial Intelligence Research Society (FLAIRS) Conference*, AAAI Press, Palo Alto: 866-867. ISBN: 9781577352341.

SFB 649 Discussion Paper Series 2014

For a complete list of Discussion Papers published by the SFB 649, please visit http://sfb649.wiwi.hu-berlin.de.

001 "Principal Component Analysis in an Asymmetric Norm" by Ngoc Mai Tran, Maria Osipenko and Wolfgang Karl Härdle, January 2014.

002 "A Simultaneous Confidence Corridor for Varying Coefficient Regression with Sparse Functional Data" by Lijie Gu, Li Wang, Wolfgang Karl Härdle and Lijian Yang, January 2014.

003 "An Extended Single Index Model with Missing Response at Random" by Qihua Wang, Tao Zhang, Wolfgang Karl Härdle, January 2014.

004 "Structural Vector Autoregressive Analysis in a Data Rich Environment: A Survey" by Helmut Lütkepohl, January 2014.

005 "Functional stable limit theorems for efficient spectral covolatility estimators" by Randolf Altmeyer and Markus Bibinger, January 2014.

006 "A consistent two-factor model for pricing temperature derivatives" by Andreas Groll, Brenda López-Cabrera and Thilo Meyer-Brandis, January 2014.

007 "Confidence Bands for Impulse Responses: Bonferroni versus Wald" by Helmut Lütkepohl, Anna Staszewska-Bystrova and Peter Winker, January 2014.

008 "Simultaneous Confidence Corridors and Variable Selection for Generalized Additive Models" by Shuzhuan Zheng, Rong Liu, Lijian Yang and Wolfgang Karl Härdle, January 2014.

009 "Structural Vector Autoregressions: Checking Identifying Long-run Restrictions via Heteroskedasticity" by Helmut Lütkepohl and Anton Velinov, January 2014.

010 "Efficient Iterative Maximum Likelihood Estimation of High-Parameterized Time Series Models" by Nikolaus Hautsch, Ostap Okhrin and Alexander Ristig, January 2014.

011 "Fiscal Devaluation in a Monetary Union" by Philipp Engler, Giovanni Ganelli, Juha Tervala and Simon Voigts, January 2014.

012 "Nonparametric Estimates for Conditional Quantiles of Time Series" by Jürgen Franke, Peter Mwita and Weining Wang, January 2014.

013 "Product Market Deregulation and Employment Outcomes: Evidence from the German Retail Sector" by Charlotte Senftleben-König, January 2014.

014 "Estimation procedures for exchangeable Marshall copulas with hydrological application" by Fabrizio Durante and Ostap Okhrin, January 2014.

015 "Ladislaus von Bortkiewicz - statistician, economist, and a European intellectual" by Wolfgang Karl Härdle and Annette B. Vogt, February 2014.

016 "An Application of Principal Component Analysis on Multivariate Time-Stationary Spatio-Temporal Data" by Stephan Stahlschmidt, Wolfgang Karl Härdle and Helmut Thome, February 2014.

017 "The composition of government spending and the multiplier at the Zero Lower Bound" by Julien Albertini, Arthur Poirier and Jordan Roulleau-Pasdeloup, February 2014.

018 "Interacting Product and Labor Market Regulation and the Impact of Immigration on Native Wages" by Susanne Prantl and Alexandra Spitz-Oener, February 2014.

This research was supported by the Deutsche Forschungsgemeinschaft through the SFB 649 "Economic Risk".

SFB 649 Discussion Paper Series 2014

For a complete list of Discussion Papers published by the SFB 649, please visit http://sfb649.wiwi.hu-berlin.de.

019 "Unemployment benefits extensions at the zero lower bound on nominal interest rate" by Julien Albertini and Arthur Poirier, February 2014.
020 "Modelling spatio-temporal variability of temperature" by Xiaofeng Cao, Ostap Okhrin, Martin Odening and Matthias Ritter, February 2014.
021 "Do Maternal Health Problems Influence Child's Worrying Status? Evidence from British Cohort Study" by Xianhua Dai, Wolfgang Karl Härdle and Keming Yu, February 2014.
022 "Nonparametric Test for a Constant Beta over a Fixed Time Interval" by Markus Reiß, Viktor Todorov and George Tauchen, February 2014.
023 "Inflation Expectations Spillovers between the United States and Euro Area" by Aleksei Netšunajev and Lars Winkelmann, March 2014.
024 "Peer Effects and Students' Self-Control" by Berno Buechel, Lydia Mechtenberg and Julia Petersen, April 2014.
025 "Is there a demand for multi-year crop insurance?" by Maria Osipenko, Zhiwei Shen and Martin Odening, April 2014.
026 "Credit Risk Calibration based on CDS Spreads" by Shih-Kang Chao, Wolfgang Karl Härdle and Hien Pham-Thu, May 2014.
027 "Stale Forward Guidance" by Gunda-Alexandra Detmers and Dieter Nautz, May 2014.
028 "Confidence Corridors for Multivariate Generalized Quantile Regression" by Shih-Kang Chao, Katharina Proksch, Holger Dette and Wolfgang Härdle, May 2014.
029 "Information Risk, Market Stress and Institutional Herding in Financial Markets: New Evidence Through the Lens of a Simulated Model" by Christopher Boortz, Stephanie Kremer, Simon Jurkatis and Dieter Nautz, May 2014.
030 "Forecasting Generalized Quantiles of Electricity Demand: A Functional Data Approach" by Brenda López Cabrera and Franziska Schulz, May 2014.
031 "Structural Vector Autoregressions with Smooth Transition in Variances – The Interaction Between U.S. Monetary Policy and the Stock Market" by Helmut Lütkepohl and Aleksei Netsunajev, June 2014.
032 "TEDAS - Tail Event Driven ASset Allocation" by Wolfgang Karl Härdle, Sergey Nasekin, David Lee Kuo Chuen and Phoon Kok Fai, June 2014.
033 "Discount Factor Shocks and Labor Market Dynamics" by Julien Albertini and Arthur Poirier, June 2014.
034 "Risky Linear Approximations" by Alexander Meyer-Gohde, July 2014
035 "Adaptive Order Flow Forecasting with Multiplicative Error Models" by Wolfgang Karl Härdle, Andrija Mihoci and Christopher Hian-Ann Ting, July 2014
036 "Portfolio Decisions and Brain Reactions via the CEAD method" by Piotr Majer, Peter N.C. Mohr, Hauke R. Heekeren and Wolfgang K. Härdle, July 2014

SFB 649, Spandauer Straße 1, D-10178 Berlin
http://sfb649.wiwi.hu-berlin.de

This research was supported by the Deutsche Forschungsgemeinschaft through the SFB 649 "Economic Risk".